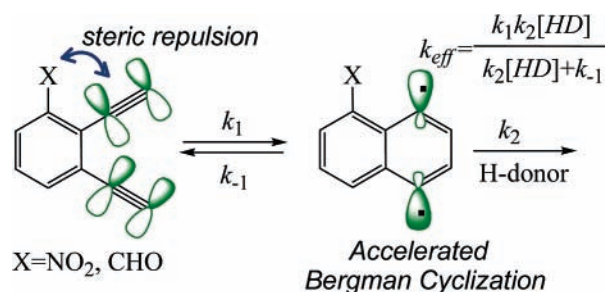


Ortho Effect in the Bergman Cyclization: Comparison of Experimental Approaches and Dissection of Cycloaromatization Kinetics

Tarek A. Zeidan, Serguei V. Kovalenko, Mariappan Manoharan, and Igor V. Alabugin*
 Department of Chemistry and Biochemistry, Florida State University, Tallahassee, Florida 32306-4390

alabugin@chem.fsu.edu

Received October 4, 2005



Four different experimental sources of kinetic information were combined to study the effect of ortho substituents on the rate of Bergman cycloaromatization. All methods confirm that the cyclization barrier is highly sensitive to the nature of the ortho substituents. However, the measured activation energies strongly depend on the choice of experimental technique: even the relative trends provided by the different methods agree with each other only in the case of acceptor substituents. Both the onset peaks and the activation energies determined by differential scanning calorimetry (DSC; either in neat enediyne or in their solutions in 10.6 M 1,4-cyclohexadiene (1,4-CHD)) strongly overestimate the reactivity of 1,2-diethynylbenzene, suggesting that DSC cannot be taken as a reliable indicator of enediyne reactivity. This discrepancy is likely to stem from the presence of side reactions with low activation barriers, especially important when the reaction is conducted in neat enediyne. On the other hand, kinetic measurements based on monitoring the concentrations of enediyne reactants and naphthalene products provide reliable general trends that include the parent benzannulated enediyne. These measurements confirm that both *ortho*-NO₂ and *ortho*-CHO substituents substantially decrease activation energies for the Bergman cyclization, supporting earlier computational predictions. A comparison of theory and experiment suggests that computations at the Moeller–Plesset second-order perturbation theory (MP2)/6-31G** level provide an excellent alternative to DFT when an accurate description of the contribution of noncovalent interactions to the activation energy is needed. Activation energies derived from k_{eff} , the effective rate constant under the pseudo-first-order approximation, depend on the 1,4-CHD concentrations. The true rate constant, k_1 , for the cyclization step and the ratio of constants for the retro-Bergman ring opening, k_{-1} , and the intermolecular H-atom abstraction, k_2 , were determined from the dependence of cycloaromatization kinetics of *ortho*- and *para*-NO₂ substituted enediynes on the concentration of 1,4-CHD.

Introduction

The Bergman cycloaromatization¹ transforms enediynes into highly reactive 1,4-dehydrobenzene (or *para*-benzyne) diradicals^{2–4} capable of abstracting two hydrogen atoms from the sugar backbone of two strands of DNA. In the case of natural enediyne antibiotics,^{5,6} this process leads to double strand

DNA cleavage and self-programmed cell death, or apoptosis. Bergman cyclization was also applied to the development of polymeric materials with valuable thermal properties⁷ and to the synthesis of polycyclic compounds.⁸ Furthermore, this reaction continues to play an important role in calibrating and developing practical theoretical methods for studies of chemical reactivity.^{9–11}

In the general sense, control over enediyne reactivity can be achieved through either strain^{12–15} or electronic effects.¹⁶ The seminal hypothesis rationalizing the influence of electronic factors was advanced by Koga and Morokuma¹⁷ who attributed the high activation energy¹⁸ of the Bergman cyclization to a strong electron repulsion between the *in-plane* occupied acetylene π orbitals. The dominating role of the *in-plane* π orbitals in the cyclization *kinetics* was particularly well-illustrated in a valence bond study of Galbraith and co-workers.¹⁹ These findings received further support in a recent natural bond orbital

(NBO) study by our group²⁰ that also found that the role of repulsion between the in-plane filled orbitals is accentuated by a parallel *decrease* in the attractive two-electron interaction between the π orbital and the π^* orbital. At the so-called “Nicolaou’s threshold” (ca. 3.2 Å),¹⁰ the attractive interaction vanishes because the in-plane π orbitals become parallel, mimicking the symmetry forbidden transition state (TS) for thermal [2 + 2] cycloaddition.²⁰ The above studies imply that electron-withdrawing substituents should promote the cyclization only when they are capable of an interaction with the in-plane π system.^{21,22} As a result, the position of the acceptor substituent becomes important. For example, Schreiner et al. demonstrated that the cyclization is accelerated by σ acceptors at the terminal acetylene atoms,²³ whereas Zaleski et al. found that such effects can be accentuated by coordination with Lewis acids in the vicinity of alkyne termini.²⁴ In contrast, Jones and Plourde showed that the progressive substitution of hydrogen atoms by halogens at the vinyl position decreases the reaction rate,²⁵ while Chen et al. found that protonation of the nitrogen atom in 3-azanedienynes increases the cyclization barrier.²⁶ Because developing radical centers do not communicate with the orthogonal π system, neither the remote substitution of the central double bond by a benzene ring (benzannelation) nor the presence of a

(1) Jones, R. R.; Bergman, R. G. *J. Am. Chem. Soc.* **1972**, *94*, 660. Bergman, R. G. *Acc. Chem. Res.* **1973**, *6*, 25. Other cycloaromatization reactions: (a) Nagata, R.; Yamanaka, H.; Okazaki, E.; Saito, I. *Tetrahedron Lett.* **1989**, *30*, 4995. (b) Myers, A. G.; Dragovich, P. S.; Kuo, E. Y. *J. Am. Chem. Soc.* **1992**, *114*, 9369. (c) Nakatani, K.; Iseo, S.; Maekawa, S.; Saito, I. *Tetrahedron Lett.* **1994**, *35*, 605. (d) Sullivan, R. W.; Coghlan, V. M.; Munk, S. A.; Reed, M. W.; Moore, H. W. *J. Org. Chem.* **1994**, *59*, 2276. (e) Toda, F.; Tanaka, K.; Sano, I.; Isozaki, T. *Angew. Chem., Int. Ed. Engl.* **1994**, *33*, 1757. (f) Nicolaou, K. C.; Skokotas, G.; Maligres, P.; Zuccarello, G.; Schweiger, E. J.; Toshima, K.; Wendeborn, S. *Angew. Chem., Int. Ed. Engl.* **1989**, *28*, 1272. (g) Engels, B.; Lennartz, C.; Hanrath, M.; Schmittel, M.; Strittmatter, M. *Angew. Chem., Int. Ed.* **1998**, *37*, 1960. (h) Schmittel, M.; Steffen, J. P.; Angel, M. A. W.; Engels, B.; Lennartz, C.; Hanrath, M. *Angew. Chem., Int. Ed.* **1998**, *37*, 1562. (i) Kawatkar, S. P.; Schreiner, P. R. *Org. Lett.* **2002**, *4*, 3643.

(2) (a) Nicolaou, K. C.; Smith, A. L. *Acc. Chem. Res.* **1992**, *25*, 497. (b) Maier, M. E.; Bosse, F.; Niestroj, A. J. *Eur. J. Org. Chem.* **1936**, *1*, 1. (c) Grissom, J. W.; Gunawardena, G. U.; Klingberg, D.; Huang, D. H. *Tetrahedron* **1996**, *52*, 6453. (d) Fallis, A. G. *Can. J. Chem.* **1999**, *77*, 159. (e) Caddick, S.; Delisser, V. M.; Doyle, V. E.; Khan, S.; Avent, A. G.; Vile, S. *Tetrahedron* **1999**, *55*, 2737. (f) Wang, K. K. *Chem. Rev.* **1996**, *96*, 207.

(3) Nicolaou, K. C.; Zuccarello, G.; Riemer, C.; Estevez, V. A.; Dai, W. M. *J. Am. Chem. Soc.* **1992**, *114*, 7360.

(4) Myers, A. G.; Dragovich, P. S. *J. Am. Chem. Soc.* **1992**, *114*, 5859.

(5) (a) *Enediyne Antibiotics as Antitumor Agents*; Borders, D. B., Doyle, T. W., Eds.; Marcel Dekker: New York, 1995. (b) *Neocarzinostatin: The Past, Present, and Future of an Anticancer Drug*; Maeda, H., Edo, K., Ishida, N., Eds.; Springer: New York, 1997.

(6) (a) Smith, A. L.; Nicolaou, K. C. *J. Med. Chem.* **1996**, *39*, 2103. (b) Paloma, L. G.; Smith, J. A.; Chazin, W. J.; Nicolaou, K. C. *J. Am. Chem. Soc.* **1994**, *116*, 3697. (c) Kappen, L. S.; Goldberg, I. H. *Biochemistry* **1983**, *22*, 4872. (d) Zein, N.; McGahren, W. J.; Morton, G. O.; Ashcroft, J.; Ellestead, G. A. *J. Am. Chem. Soc.* **1989**, *111*, 6888. (e) De Voss, J. J.; Townsend, C. A.; Ding, W. D.; Morton, G. O.; Ellestad, G. A.; Zein, N.; Tabor, A. B.; Schreiber, S. L. *J. Am. Chem. Soc.* **1990**, *112*, 9669. (f) Hangeland, J. J.; Voss, J. J.; Heath, J. A.; Townsend, C. A.; Ding, W. D.; Ashcroft, J. S.; Ellestad, G. A. *J. Am. Chem. Soc.* **1992**, *114*, 9200. (g) Dedon, P. C.; Salzberg, A. A.; Xu, J. H. *Biochemistry* **1993**, *32*, 3617. (h) Christner, D. F.; Frank, B. L.; Kozarich, J. W.; Stubbe, J.; Golik, J.; Doyle, T. W.; Rosenberg, I. E.; Krishnan, B. *J. Am. Chem. Soc.* **1992**, *114*, 8763. (i) Sugiura, Y.; Shiraki, T.; Konishi, M.; Oki, T. *Proc. Natl. Acad. Sci. U.S.A.* **1990**, *87*, 3831. (j) Shiraki, T.; Uesugi, M.; Sugiura, Y. *Biochem. Biophys. Res. Commun.* **1992**, *188*, 584. (k) Shiraki, T.; Sugiura, Y. *Biochemistry* **1990**, *29*, 9795. (l) Sugiura, Y.; Arakawa, T.; Uesugi, M.; Shiraki, T.; Ohkuma, H.; Konishi, M. *Biochemistry* **1991**, *30*, 2989. (m) Matsumoto, T.; Okuno, Y.; Sugiura, Y. *Biochem. Biophys. Res. Commun.* **1993**, *195*, 659. (n) Xu, Y.; Zhen, Y. S.; Goldberg, I. H. *Biochemistry* **1994**, *33*, 5947.

(7) Chen, X.; Tolbert, L. M.; Hess, D. W.; Henderson, C. *Macromolecules* **2001**, *34*, 4104. Shah, H. V.; Babb, D. A.; Smith, D. W., Jr. *Polymer* **2000**, *41*, 4415. John, J. A.; Tour, J. M. *J. Am. Chem. Soc.* **1994**, *116*, 5011.

(8) Bowles, D. M.; Palmer, G. J.; Landis, C. A.; Scott, J. L.; Anthony, J. E. *Tetrahedron* **2001**, *57*, 3753. Bowles, D. M.; Anthony, J. E. *Org. Lett.* **2000**, *2*, 85.

(9) (a) Scheiner, A. C.; Schaefer, H. F., III; Liu, B. *J. Am. Chem. Soc.* **1989**, *111*, 3118. (b) Nicolaidis, A.; Borden, W. T. *J. Am. Chem. Soc.* **1993**, *115*, 11951. (c) Lindh, R.; Persson, B. J. *J. Am. Chem. Soc.* **1994**, *116*, 4963. (d) Lindh, R.; Lee, T. J.; Bernhardtsson, A.; Persson, B. J.; Karlström, G. *J. Am. Chem. Soc.* **1995**, *117*, 7186. (e) Kraka, E.; Cremer, D.; Bucher, G.; Wandel, H.; Sander, W. *Chem. Phys. Lett.* **1997**, *268*, 313. (f) Lindh, R.; Ryde, U.; Schütz, M. *Theor. Chem. Acc.* **1997**, *97*, 203. (g) Chen, W. C.; Chang, N. W.; Yu, C. H. *J. Phys. Chem. A* **1998**, *102*, 2584. (h) McMahon, R. J.; Halter, R. J.; Fimmen, R. L.; Wilson, R. J.; Peebles, S. A.; Kuczowski, R. L.; Stanton, J. F. *J. Am. Chem. Soc.* **2000**, *122*, 939.

(10) Schreiner, P. R. *J. Am. Chem. Soc.* **1998**, *120*, 4184. Schreiner, P. R. *J. Chem. Soc., Chem. Commun.* **1998**, 483.

(11) Cramer, C. J.; Nash, J. J.; Squires, R. R. *Chem. Phys. Lett.* **1997**, *277*, 311. Cramer, C. J.; Squires, R. R. *J. Phys. Chem. A* **1997**, *101*, 9191. Wierschke, S. G.; Nash, J. J.; Squires, R. R. *J. Am. Chem. Soc.* **1993**, *115*, 11958. Johnson, W. T. G.; Sullivan, M. B.; Cramer, C. J. *Int. J. Quantum Chem.* **2001**, *85*, 492. Johnson, W. T. G.; Cramer, C. J. *J. Phys. Org. Chem.* **2001**, *14*, 597. Cramer, C. J.; Thompson, J. J. *Phys. Chem. A* **2001**, *105*, 2091. Kraka, E.; Cremer, D. *J. Comput. Chem.* **2001**, *22*, 216.

(12) Incorporation of the enediyne unit into a strained 9- or 10-membered ring was shown to facilitate the reaction through ground-state destabilization. For the experimental work, see: (a) Nicolaou, K. C.; Zuccarello, G.; Ogawa, Y.; Schweiger, E. J.; Kumazawa, T. *J. Am. Chem. Soc.* **1988**, *110*, 4866. (b) Iida, K.; Hiram, M. *J. Am. Chem. Soc.* **1995**, *117*, 8875.

(13) For a theoretical analysis of the strain effects on the cyclization, see: (a) Snyder, J. P. *J. Am. Chem. Soc.* **1989**, *111*, 7630. (b) Snyder, J. P.; Tipson, G. E. *J. Am. Chem. Soc.* **1990**, *112*, 4040. (c) Snyder, J. P. *J. Am. Chem. Soc.* **1990**, *112*, 5367.

(14) Kraka, E.; Cremer, D. *J. Am. Chem. Soc.* **1994**, *116*, 4929.

(15) The cyclization can also be controlled by the release of strain in the TS: (a) Magnus, P.; Carter, P.; Elliott, J.; Lewis, R.; Harling, J.; Pitterna, T.; Bauta, W. E.; Fortt, S. *J. Am. Chem. Soc.* **1992**, *114*, 2544.

(16) For the most recent review, see: Rawat, D. S.; Zaleski, J. M. *Synlett* **2004**, 293.

(17) Koga, N.; Morokuma, K. *J. Am. Chem. Soc.* **1991**, *113*, 1907.

(18) (a) Roth, W. R.; Hopf, H.; Horn, C. *Chem. Ber.* **1994**, *127*, 1765.

(b) Wenthold, P. G.; Squires, R. R. *J. Am. Chem. Soc.* **1994**, *116*, 6401.

(19) Galbraith, J. M.; Schreiner, P. R.; Harris, N.; Wei, W.; Wittkopp, A.; Shaik, S. *Chem.—Eur. J.* **2000**, *6*, 1446.

(20) Alabugin, I. V.; Manoharan, M. *J. Phys. Chem. A* **2003**, *107*, 3363.

(21) Schmittel, M.; Kiau, S. *Chem. Lett.* **1995**, 953.

(22) Maier, M. E.; Greiner, B. *Liebigs Ann. Chem.* **1992**, 855.

(23) Jones, G. B.; Warner, P. M. *J. Am. Chem. Soc.* **2001**, *123*, 2134. König, B.; Pitsch, W.; Klein, M.; Vasold, R.; Prall, M.; Schreiner, P. R. *J. Org. Chem.* **2001**, *66*, 1742. Prall, M.; Wittkopp, A.; Fokin, A. A.; Schreiner, P. R. *J. Comput. Chem.* **2001**, *22*, 1605. Chemistry of metalloenedienynes: Benites, P. J.; Rawat, D. S.; Zaleski, J. M. *J. Am. Chem. Soc.* **2000**, *122*, 7208. Rawat, D. S.; Zaleski, J. M. *J. Am. Chem. Soc.* **2001**, *123*, 9675.

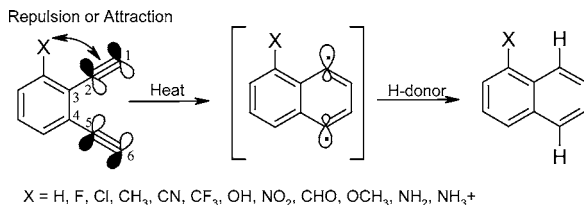
Coalter, N. L.; Concolino, T. E.; Streib, W. E.; Hughes, C. G.; Rheingold, A. L.; Zaleski, J. M. *J. Am. Chem. Soc.* **2000**, *122*, 3112. Chandra, T.; Pink, M.; Zaleski, J. M. *Inorg. Chem.* **2001**, *40*, 5878. Rawat, D. S.; Zaleski, J. M. *Synth. Commun.* **2002**, *32*, 1489. Rawat, D. S.; Benites, P. J.; Incarvito, C. D.; Rheingold, A. L.; Zaleski, J. M. *Inorg. Chem.* **2001**, *40*, 1846.

Schmitt, E. W.; Huffman, J. C.; Zaleski, J. M. *Chem. Commun.* **2001**, 167. Rawat, D. S.; Zaleski, J. M. *Chem. Commun.* **2000**, 2493. Benites, P. J.; Lato, S. M.; Ellington, A. D.; Zaleski, J. M. *J. Inorg. Biochem.* **1999**, *74*, 75.

(24) Bhattacharyya, S.; Pink, M.; Baik, M. H.; Zaleski, J. M. *Angew. Chem., Int. Ed.* **2005**, *44*, 592.

(25) Jones, G. B.; Plourde, G. W. *Org. Lett.* **2000**, *2*, 1757.

(26) Hoffner, J.; Schottelius, M. J.; Feichtinger, D.; Chen, P. *J. Am. Chem. Soc.* **1998**, *120*, 376.

SCHEME 1. Bergman Cyclization of Ortho-Substituted Benzannelated Eneidyne


substituent at the aromatic ring strongly affects the cyclization barrier in benzannelated eneidyne.²⁷

Nevertheless, the rates of cyclizations of benzannelated eneidyne were reported to be slower and more sensitive to hydrogen-donor (HD) concentration than in the case of comparable acyclic eneidyne.²⁸ This effect was attributed to the faster retro-Bergman ring opening accentuated by the decreased reactivity of *p*-benzynes toward hydrogen abstraction.^{29,30} The retro-Bergman ring opening of benzannelated eneidyne is fast because the loss of aromatic stabilization upon the transformation of naphthalene to benzene is less than in the process of the opening of the benzene ring in the parent *p*-benzyne. Although the importance of the *out-of-plane* interactions increases progressively after the TS, the low sensitivity of reaction kinetics to substituent effects is one of the largest challenges to efficient control and rational design of cycloaromatization reactions.

Russell and co-workers have shown that the influence of para substituents on the rates of disappearance of benzannelated eneidyne is mainly transmitted through the field effect and, thus, is relatively small.²⁷ Recently, our group confirmed these findings computationally and suggested that ortho substituents that are spatially close to the eneidyne moiety can control the rate of Bergman cyclization more efficiently (Scheme 1).³¹ Depending on the substituent, their interaction with the eneidyne moiety and adjacent radical center in the *p*-benzyne can be either attractive (H bonding) or repulsive (steric). The third mechanism for the ortho effect is different and is based on the interception of the *p*-benzyne diradical by intramolecular H abstraction, which renders the cyclization step irreversible.³²

In particular, the NO₂, CF₃, *syn*-CHO, and *syn*-OMe groups were predicted to decrease the activation energy for the Bergman

cyclization by destabilizing reactants through steric repulsion between the ortho substituent and the in-plane acetylenic orbitals (Figure 1). This interaction becomes less significant in the TS when the acetylene moiety is bent away from the ortho functional group. As a result, the TS and the product are destabilized to a lesser extent than the starting material and the activation barrier is decreased through the classic *steric-assistance* mechanism.³³ The steric nature of this effect is clear from the comparison with the respective para isomers. For example, the *ortho*-nitroeneidyne is *less stable* than the para isomer by 5.8 kcal/mol at the B3LYP/6-31G** level, as illustrated in Figure 1. The difference in stability decreases to 2.8 kcal/mol in the TS and to 2.0 kcal/mol in the product, accounting for the 3 kcal/mol decrease in the cyclization barrier and the 3.8 kcal/mol decrease in the reaction endothermicity.

In contrast, such substituents as CH₃, NH₂, NH₃⁺, and *syn*-OH are predicted to stabilize respective *ortho*-eneidyne relative to their para isomers because of a hydrogen-bond formation between the X–H moiety and the in-plane π bond.³⁴ Interestingly, both B3LYP computations and BLYP computations predict that this stabilization will *decrease* in the TS for all of these neutral substrates and *increase* for the positively charged ammonium group, accounting for the barrier decrease in the latter case.³¹ Although this difference in the dynamics of such noncovalent interactions between the neutral and the charged moieties can be rationalized through a larger electrostatic contribution to H bonding of cationic species, such subtle variations along with the known deficiencies of DFT in the description of noncovalent interactions³⁵ do suggest that such DFT predictions should be taken with caution until they are verified experimentally.

The aldehyde case is even more complicated. Depending on the orientation of the carbonyl group, this eneidyne may exist as two conformers that have different barriers for the transformation. B3LYP, BLYP, and Moeller–Plesset second-order perturbation theory (MP2) calculations with the 6-31G** basis set uniformly predict the anti conformer of the starting material to be 2.4–2.8 kcal/mol more stable than the *syn* isomer. Both conformers are predicted to be more reactive than *para*-NO₂ substituted eneidyne by DFT: the *syn* conformer by about 3 kcal/mol and the anti conformer by about 2 kcal/mol. The Curtin–Hammett analysis suggests that the cyclization should mostly proceed through the more stable anti conformer, with the overall decrease in the barrier on the order of 2 kcal/mol. Interestingly, computational comparison with the respective para isomer suggests that a decrease in the cyclization barrier in the case of the anti isomer stems both from reactant destabilization and from TS stabilization, whereas the Bergman cyclization of the *syn* isomer is accelerated by the steric assistance (similar to the effect of the NO₂ moiety).

Steric compression of the eneidyne moiety by ortho substituents is further illustrated in Figure 2, which clearly shows that steric destabilization is accompanied by a decrease in the distance between the terminal acetylenic carbons (C1C6).

In this paper, we test our computational predictions with experimental studies designed to determine whether ortho substituents are capable of decreasing the activation energy of the Bergman cyclization. To obtain reliable results, we will

(27) Choy, N.; Kim, C. S.; Ballester, C.; Artigas, L.; Diez, C.; Lichtenberg, F.; Shapiro, J.; Russell, K. C. *Tetrahedron Lett.* **2000**, *41*, 6955.

(28) Semmelhack, M. F.; Neu, T.; Foubelo, F. *J. Org. Chem.* **1994**, *59*, 5038. Kaneko, T.; Takahashi, M.; Hirama, M. *Tetrahedron Lett.* **1999**, *40*, 2015. For a recent discussion, see: Semmelhack, M. F.; Sarpong, R. *J. Phys. Org. Chem.* **2004**, *17*, 807.

(29) For the decrease in retro-Bergman barrier, see: Haberhauer, G.; Gleiter, R. *J. Am. Chem. Soc.* **1999**, *121*, 4664. Koseki, S.; Fujimura, Y.; Hirama, M. *J. Phys. Chem. A* **1999**, *103*, 7672. Stahl, F.; Moran, D.; Schleyer, P. v. R.; Prall, M.; Schreiner, P. R. *J. Org. Chem.* **2002**, *67*, 1453.

(30) Diradicals are less reactive than the respective monoradicals because of the loss of TB interaction between the two radical centers in the first hydrogen abstraction step. For *p*-benzyne, the difference in the barriers of the first and the second H abstractions from methanol is about 1.6 kcal/mol at the CASPT2N/6-31G**//CAS/3-21G level: Logan, C. F.; Chen, P. *J. Am. Chem. Soc.* **1996**, *118*, 2113. See also: Schottelius, M. J.; Chen, P. *J. Am. Chem. Soc.* **1996**, *118*, 4896. For a more detailed description of TB interactions, see: Hoffman, R.; Imamura, A.; Hehre, W. J. *J. Am. Chem. Soc.* **1968**, *90*, 1499. Hoffman, R. *Acc. Chem. Res.* **1971**, *4*, 1. Squires, R. R.; Cramer, C. J. *J. Phys. Chem. A* **1998**, *102*, 9072. For the theoretical analysis of the TB interaction in cyclohexyl cations, see: Alabugin, I. V.; Manoharan, M. *J. Org. Chem.* **2004**, *69*, 9011.

(31) Alabugin, I. V.; Manoharan, M.; Kovalenko, S. V. *Org. Lett.* **2002**, *4*, 1119.

(32) Zeidan, T. A.; Manoharan, M.; Alabugin, I. V. *J. Org. Chem.* Preceding paper in this issue.

(33) Eliel, E. L.; Wilen, S. H.; Doyle, M. P. *Basic Organic Stereochemistry*; Wiley-Interscience: New York, 2001; p 459.

(34) For NBO analysis of these H bonds, see ref 31.

(35) Müller-Dethlefs, K.; Hobza, P. *Chem. Rev.* **2000**, *100*, 143.

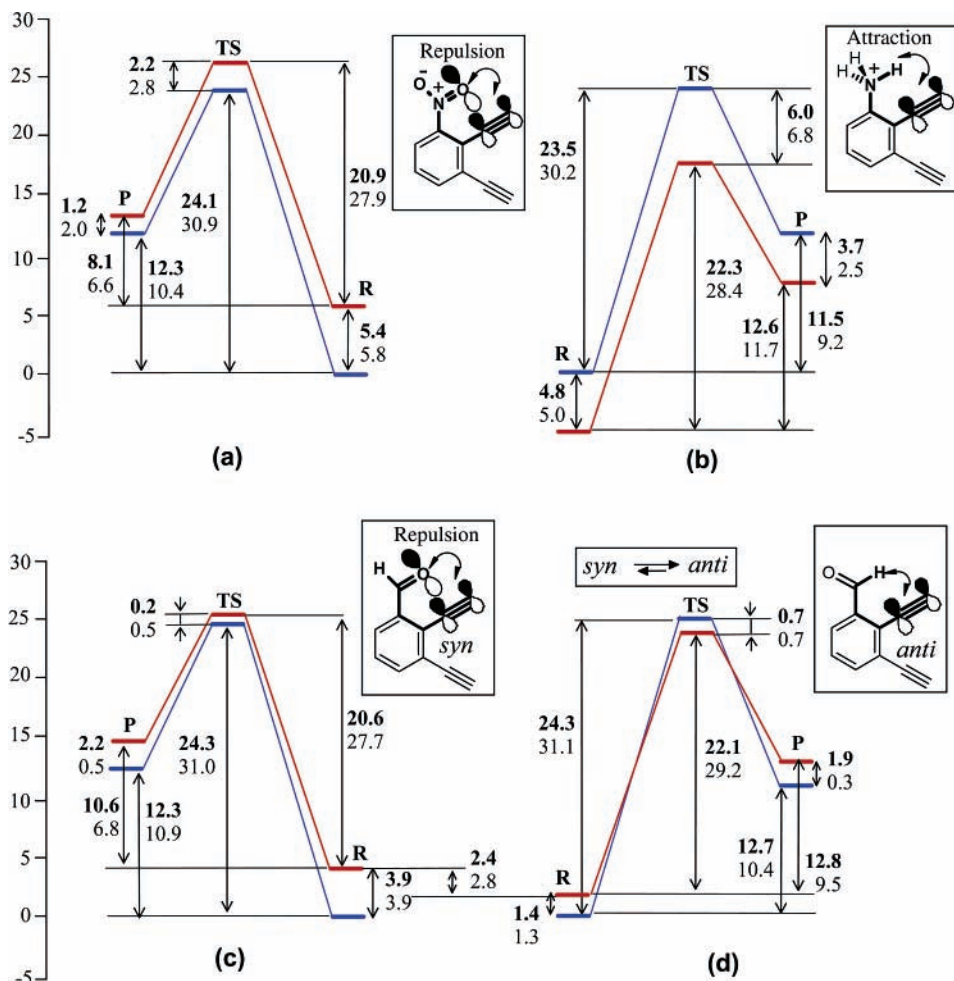


FIGURE 1. Steric-assistance (a, c) and H-bonding (b, d) mechanisms for the “ortho” effect. Energy profile for the para isomer is given in solid blue lines, whereas data for the ortho isomer are shown in solid red lines. Calculations were performed at the BLYP/6-31G** (in bold) and B3LYP/6-31G** levels. **P** stands for products, and **R** stands for reactants.

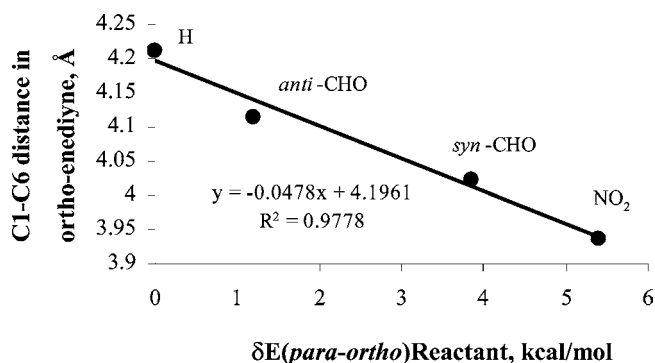


FIGURE 2. Correlation between the C1C6 distance and the relative energies of ortho and para isomers of substituted benzannelated enediyne.

critically evaluate several common experimental approaches. Such an evaluation is necessary because the available body of literature on the Bergman cyclization kinetics is highly heterogeneous and, thus, a direct comparison of related results from different groups is often problematic. To avoid complications that exist when other reactions compete with the Bergman cyclization (vide infra), we will concentrate on the Bergman cycloaromatization of enediyne with acceptor substituents, where side reactions are minimized. This choice will allow us

to compare the accuracy of commonly used kinetic methods and to show that the complex thermal reactivity of enediyne requires more detailed kinetic analysis of other steps in the cycloaromatization cascade. As a result, both experiment and theory are refined, and a more balanced description of such processes is achieved.

Results and Discussions

Synthesis of Enediyne. The model enediyne was synthesized using standard literature procedures outlined in Scheme 2. The aromatic dihalides or ditriflates³⁶ were coupled with trimethylsilylacetylene under Sonogashira conditions.³⁷ In addition to the ortho-substituted substrates, we prepared two reference compounds: the parent benzannelated enediyne **1** and the *para*-NO₂ enediyne **3**. Treatment of the trimethylsilyl (TMS)-protected enediyne with a base (typically 1 N NaOH) afforded ortho-substituted benzannelated enediyne in good yields. Bergman cyclizations of enediyne on a preparative scale

(36) Powell, N. A.; Rychnovsky, S. D. *Tetrahedron Lett.* **1996**, *37*, 7901.

(37) (a) Sonogashira, K.; Tohda, Y.; Hagihara, N. *Tetrahedron Lett.* **1975**, 4467. (b) Sonogashira, K. In *Metal-Catalyzed Reactions*; Diederich, F., Stang, P. J., Eds.; Wiley-VCH: New York, 1998. (c) Stang, P. J. In *Modern Acetylene Chemistry*; Diederich, F., Ed.; VCH: Weinheim, Germany, 1995. (d) Tykwinski, R. R. *Angew. Chem., Int. Ed.* **2003**, *42*, 1566.

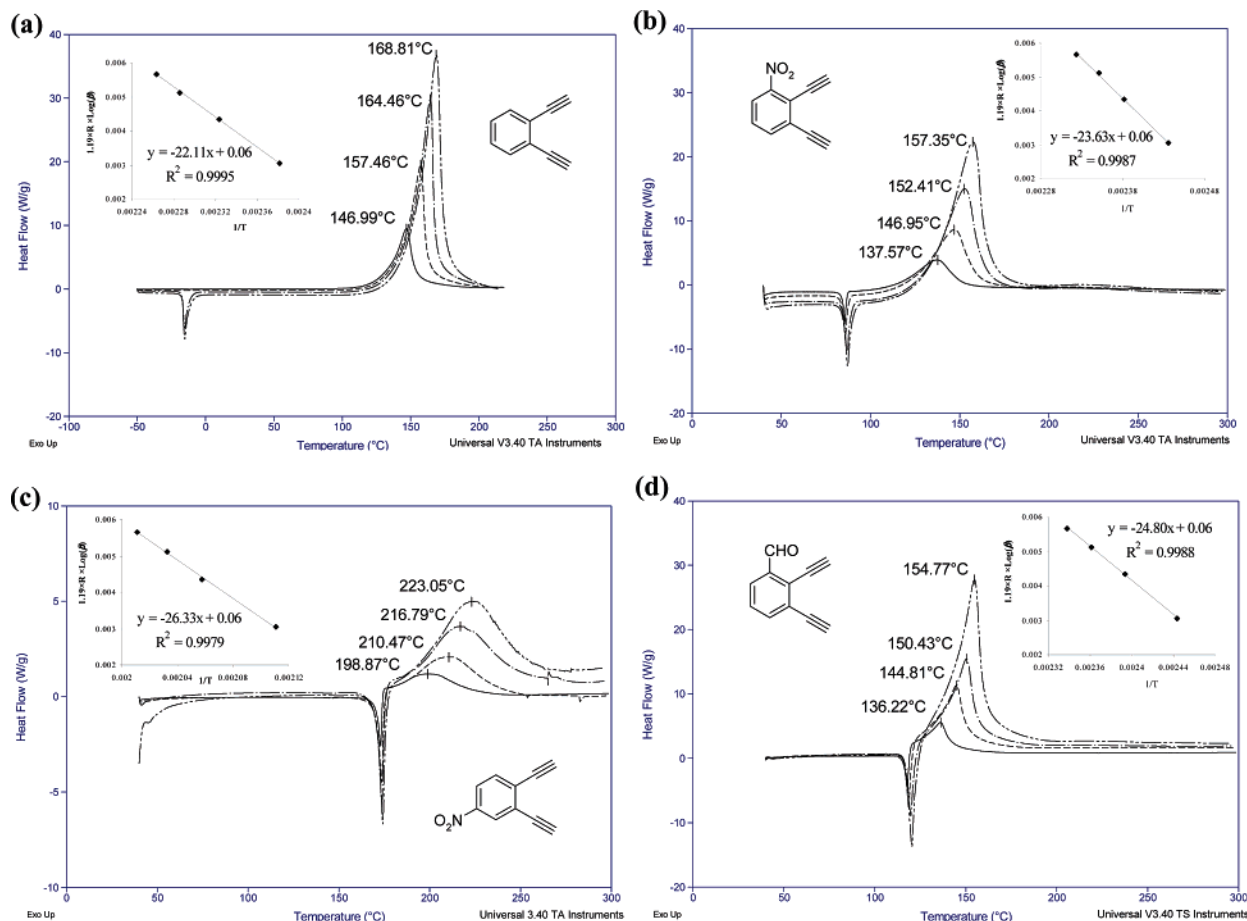
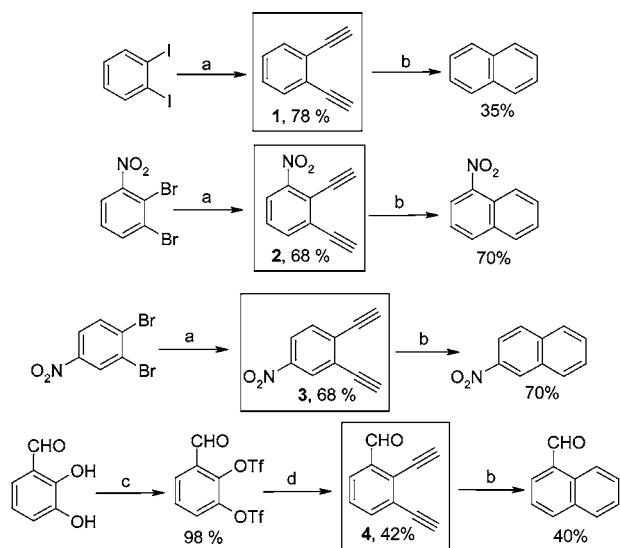


FIGURE 3. DSC scans of neat benzannulated enediynes at a heating rate of 5, 10, 15, and 20 °C/min and the nonrefined activation energies⁴⁵ (insets) for (a) 1,2-diethynylbenzene, (b) 2,3-diethynyl-1-nitrobenzene, (c) 3,4-diethynyl-1-nitrobenzene, and (d) 2,3-diethynyl-1-formylbenzene.

SCHEME 2. Synthesis of Ortho-Substituted Benzannulated Enediynes



Reagents and conditions: (a) 1. Pd(PPh₃)₂Cl₂, (i-Pr)₂NH, Cu(I), HCCSiMe₃ and 2. NaOH, MeOH (b) PhCl, 1,4-cyclohexadiene (c) Tf₂O, Pyridine, CH₂Cl₂ (d) 1. Pd(PPh₃)₂Cl₂, Et₃N/DMF, HCCSiMe₃, 2. MeOH, K₂CO₃

were performed in Pyrex glass tubes containing a solution of the enediynes and 1,4-cyclohexadiene (1,4-CHD) in chlorobenzene at 0.10 and 10.0 M concentration of enediynes and 1,4-CHD, respectively.

Differential Scanning Calorimetry (DSC) Analysis. An initial comparison of the thermal reactivities of the ortho-substituted enediynes was carried out using DSC, the method which has rapidly gained popularity as a way to scan enediynes for increased reactivity. The quickest but also the crudest way to use DSC is based on the onset of the exothermic peak.³⁸ Results of these measurements are given in Figure 3. Contrary to the expectations based on the computational analysis, the onset temperature for 1,2-diethynylbenzene is only 9–10 °C higher than that for the *ortho*-NO₂ and *ortho*-CHO substituted enediynes and 60 °C lower than for the *para*-NO₂ enediynes.³⁹ The latter observation is in direct conflict with the experimental trend determined by Russell and co-workers in solution.²⁷ Interestingly, the *ortho*-CHO and *para*-NO₂ enediynes react immediately after melting. These observations suggest that the solid state may impose constraints on reactivity.⁴⁰ Considering all of the above, it is clear that trends in the onset DSC temperatures of pure enediynes cannot be used as a universal criterion of the relative reactivity.

(38) For reviews, see ref 16 and Basak, A.; Mandal, S.; Bag, S. S. *Chem. Rev.* **2003**, *103*, 4077. Perera, K. P. U.; Shah, H. V.; Foulger, S. H.; Smith, D. W., Jr. *Thermochim. Acta* **2002**, *388*, 371.

(39) Onsets of the exothermic peaks for enediynes at different heating rates (5, 10, 15, and 20 °C) are 132, 142, 149, and 151 °C (1), 114, 123, 133, and 129 °C (2), 193, 203, 210, and 217 °C (3), and 127, 137, 142, and 147 °C (4).

(40) For an example of the crystal control of photochemical reactivity, see: Zimmerman, H. E.; Alabugin, I. V.; Smolenskaya, V. N. *Tetrahedron* **2000**, *56*, 6821 and references therein.

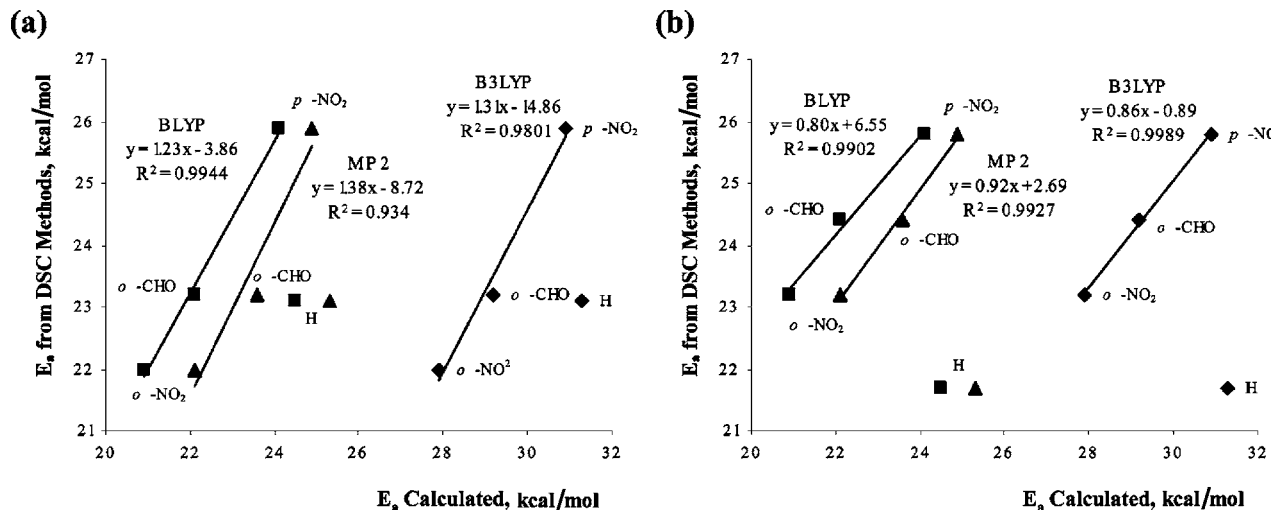


FIGURE 4. Correlation between activation energies calculated using MP2, B3LYP, and BLYP levels⁷⁹ with the 6-31G(d,p) basis set and activation energies determined using the DSC method of benzannelated enediynes in 1,4-CHD bearing electron acceptor groups in the ortho position: (a) neat 1,4-CHD solution and (b) neat benzannelated enediynes. 1,2-Diethynylbenzene is not included in these correlations.

To evaluate the effect of crystalline restraints, we performed the DSC analysis in neat 1,4-CHD (see Supporting Information for the plots). In these experiments, 50 μ L portions of the stock solutions of enediynes in 1,4-CHD were sealed in “high volume pans”⁴¹ under argon in a glovebox. DSC scans were carried out under similar conditions as described above but with a maximum temperature of 250 $^{\circ}$ C (see Supporting Information).⁴² In all cases, reaction exotherms were observed after the initial endothermic response caused by the partial solvent vaporization. After each DSC run, the samples were tested by TLC and found to contain the corresponding naphthalenes as the major products. However, the trends for the onset peaks were similar to those observed for the neat enediynes.

More detailed kinetic information can be obtained from the combination of the DSC analysis with the ASTM E 698 thermal stability method (insets).⁴³ The ASTM E 698 analysis requires three or more experiments at different heating rates and, under the assumption of a first-order kinetic model, provides activation energies for the reaction.⁴⁴ We carried out the nonisothermal DSC scans for neat enediynes and their solutions in 1,4-CHD at four different heating rates (5, 10, 15, and 20 $^{\circ}$ C). As expected, an increase in the heating rate shifts the peaks of the exotherms to higher temperatures. The activation energies are then obtained by plotting $\ln(\epsilon)$ versus $1/RT$, where ϵ is the peak maximum of the exotherm.⁴⁵

Again, the anomalously low DSC activation energy for 1,2-diethynylbenzene disagrees with the experimental results of Grissom et al.⁴⁶ and Russell et al.²⁷ and with the computationally predicted trends. This discrepancy is likely to stem from side

reactions with low activation barriers that become especially important when the reaction is conducted in neat enediyne. The cumulative heat release does not provide individual information about the evolution of the chemical species involved in specific processes which may coexist competing with the Bergman cyclization. Chain radical cyclizations involving the addition of *p*-benzynes or other radical intermediates to the acetylene moieties or to 1,4-CHD are the most likely candidates for such processes.^{47–49} Moreover, the shape of the 1,2-diethynylbenzene exotherm is indicative of an autocatalytic reaction, which agrees very well with the chain radical process.⁵⁰ These observations also explain the relatively low (35%) yield for the naphthalene product, even in the presence of a large excess of 1,4-CHD. Similar to the first set of DSC experiments, higher heating rates resulted in the sharpening of the exothermic peak and the shifting of its maximum to higher temperatures. As a result of the lower reactivity of the *para*-NO₂ enediyne, lower heating rates were used to ensure the completion of the exothermic peak before the maximum operational temperature of 250 $^{\circ}$ C of the high volume pans was reached.

The DSC activation energies for the cyclization of three enediynes with acceptor substituents are in excellent agreement with the earlier DFT estimates. Correlations given in Figure 4 suggest that BLYP values are closer to the experimental DSC data. However, the difference is small and B3LYP is at least as good as BLYP (or better) in predicting *relative trends* in the reactivity of this family of substituted enediynes. However, it is clear that the case of X = H is an outlier. One can attribute

(41) High volume pans are aluminum pans usually used for liquid samples. They were purchased from TA Instrument, Inc.

(42) As a result of high pressure produced inside the DSC high volume pans caused by heating the 1,4-CHD, the maximum temperature reached was 250 $^{\circ}$ C.

(43) *Standard Test Method for Arrhenius Kinetic Constants for Thermally Unstable Materials (ANSI/ASTM E 698–99) ASTM Book of Standards*; ASTM: Philadelphia, PA, 2000; Vol. 14.02, pp 299–305.

(44) Ozawa, T. J. *Thermal Anal.* **1970**, *2*, 301.

(45) Activation energies determined from the plots in Figure 3 are refined according to the ASTM E 698–99 protocol (see ref 42). The refined activation energies are reported in Table 4.

(46) Grissom, J. W.; Calkins, T. L.; McMillen, H. A.; Jiang, Y. H. *J. Org. Chem.* **1994**, *59*, 5833.

(47) (a) König, B.; Pitsch, W.; Klein, M.; Vasold, R.; Prall, M.; Schreiner, P. R. *J. Org. Chem.* **2001**, *66*, 1742. (b) Kovalenko, S. V.; Peabody, S.; Manoharan, M.; Clark, R. J.; Alabugin, I. V. *Org. Lett.* **2004**, *6*, 2457. Peabody, S. W.; Breiner, B.; Kovalenko, S. V.; Alabugin, I. V. *Org. Biomol. Chem.* **2005**, *3*, 218. (c) Johnson, J. P.; Bringley, D. A.; Wilson, E. E.; Lewis, K. D.; Beck, L. W.; Matzger, A. J. *J. Am. Chem. Soc.* **2003**, *125*, 14708.

(48) Rule, J. D.; Wilson, S. R.; Moore, J. S. *J. Am. Chem. Soc.* **2003**, *125*, 12992.

(49) For theoretical analysis, see: (a) Alabugin, I. V.; Manoharan, M. *J. Am. Chem. Soc.* **2005**, *127*, 9534. (b) Alabugin, I. V.; Manoharan, M. *J. Am. Chem. Soc.* **2005**, *127*, 12583.

(50) Jacobs, P. W.; Tompkins, F. C. In *Chemistry of the Solid State*; Garner, W. E., Ed.; Academic Press: New York, 1955; p 184. Also see: Bou-Diab, L.; Fierz, H. *J. Hazard. Mater.* **2002**, *93*, 137.

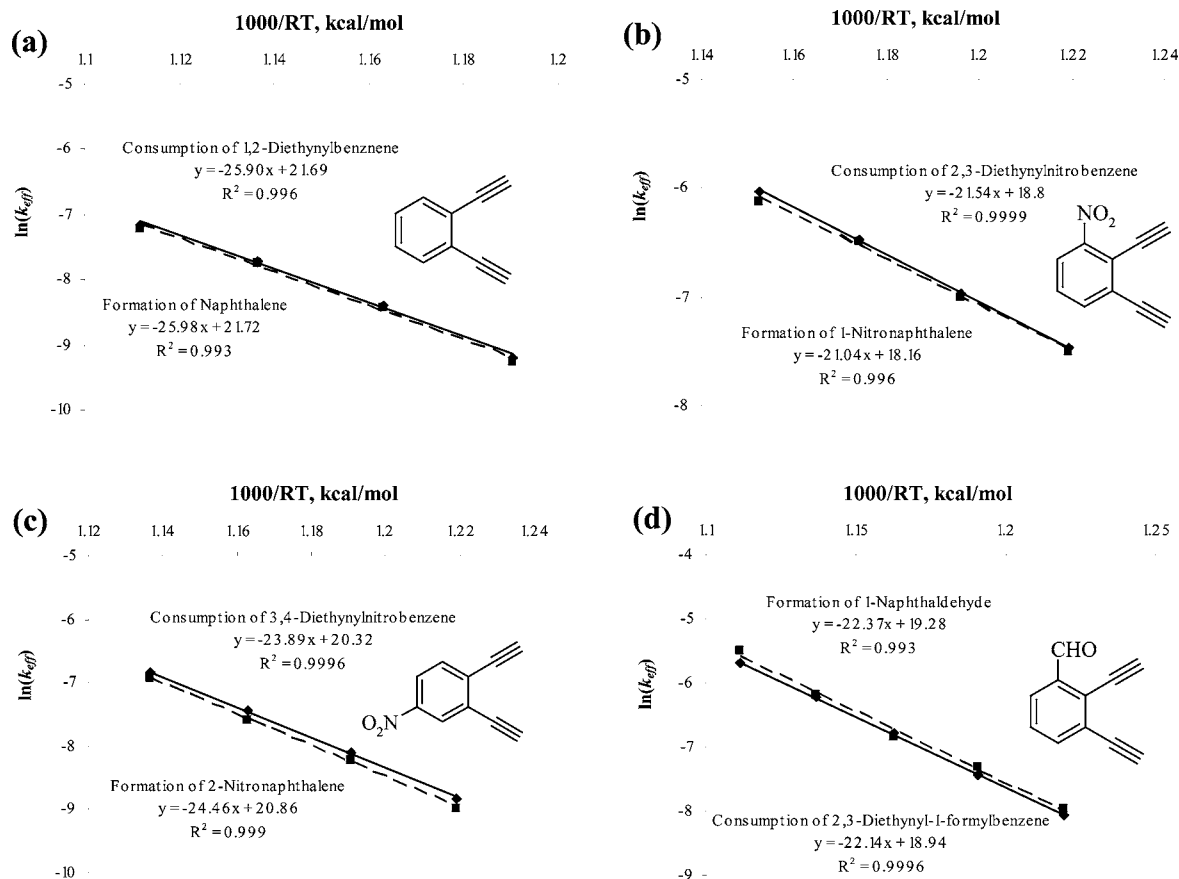


FIGURE 5. Arrhenius plots for the disappearance of ortho-substituted enediynes (solid line) and the appearance of the corresponding naphthalenes (dashed lines). (a) 1,2-diethynylbenzene, (b) 2,3-diethynyl-1-nitrobenzene, (c) 3,4-diethynyl-1-nitrobenzene, and (d) 2,3-diethynyl-1-formylbenzene.

this difference to the greater thermal stability of acceptor enediynes and to their lesser propensity to participate in radical processes.⁴⁷ Interestingly, the presence of 1,4-CHO does not improve the quality of the correlation, and in both cases, the slope of the correlation between experimental and theoretical barriers is significantly different from 1.

The anomalous position of the unsubstituted enediyne suggests that DSC is not universally reliable for kinetic studies of the Bergman cyclization. Only in the cases of kinetically simple and chemically efficient processes within a family of related compounds (e.g., enediynes with acceptor substituents) can such comparisons be justifiable. Thus, we carried out a more thorough kinetic analysis on the basis of following the concentrations of the reactants and the products during the cycloaromatization process.

Effective Rate Constants and Activation Energies for the Cyclization of Ortho-Substituted Enediynes. The conditions described by Grissom et al. (freeze/pump/thaw degassed solutions, sealed capillaries, and chlorobenzene as a solvent, see Experimental Section)⁵¹ were used to allow a comparison with the earlier literature. Effective rate constants for the disappearance of ortho-substituted enediynes and the appearance of the corresponding naphthalene products were measured at different temperatures. The consumption of enediynes followed the pseudo-first-order exponential dependence of eq 1 (Figure S1

in Supporting Information). Similarly, the appearance of naphthalene products followed a pseudo-first-order kinetic behavior. The effective rate constants, k_{eff} , for the formation of the Bergman products were determined by fitting the data to eq 2, which normalizes the formation of the product to the observed reaction yield,⁵²

$$[A] = [A]_0 e^{-k_{\text{eff}} t} \quad (1)$$

$$\ln(X) = \ln\left(\frac{[P_\infty]}{[P_\infty] - [C]}\right) = k_{\text{eff}} t \quad (2)$$

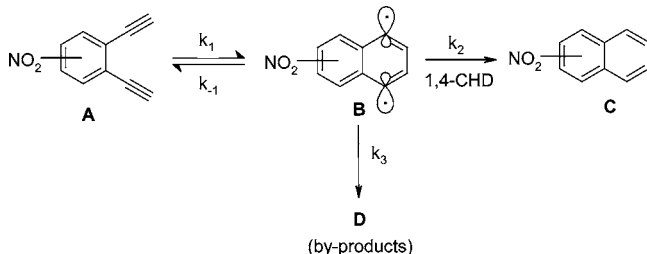
where $[A]_0$ is the initial concentration of the enediynes, $[P_\infty]$ is the yield of the product, and $[A]$ and $[C]$ are the concentrations of the enediynes and the naphthalenes at time t , respectively.⁵³ Arrhenius plots based on the pseudo-first-order effective rate constants at greater than or equal to four different temperatures provided the activation energies given in Figure 5.

Unlike the DSC data, all of the above results are consistent with the theoretically predicted trends. Although the rates of the CHO–naphthalene formation have the largest margin of error as a result of the increased formation of byproducts,^{54,55}

(52) The use of $[P_\infty]$ instead of $[A]_0$ in eq 2 eliminates the nonlinearity of the fit at higher conversions and has an effect on the values of the measured Arrhenius barriers.

(53) Some of the data points at long reaction times had to be discarded because the reaction becomes less efficient at the low concentration levels of the starting enediynes and errors in integrating the areas of the naphthalene products increase substantially. See Supporting Information for complete details of kinetic experiments.

(51) (a) Grissom, J. W.; Calkins, T. L. *J. Org. Chem.* **1993**, *58*, 5422. (b) Grissom, J. W.; Calkins, T. L.; McMillen, H. A.; Jiang, Y. H. *J. Org. Chem.* **1994**, *59*, 5833. (c) Grissom, J. W.; Gunawardena, G. U. *Tetrahedron Lett.* **1995**, *36*, 4951.

SCHEME 3. Kinetically Important Steps Involved in the Cycloaromatization Cascade


it is clear that both *ortho*-CHO and *ortho*-NO₂ substrates have increased reactivity relative to *para*-NO₂ enediyne and 1,2-diethynylbenzene (effective rate constants are given in Supporting Information). Among the two reference compounds, the *para*-nitroenediynes is slightly more reactive, as shown earlier by Russell and co-workers.²⁷ When eq 2 is used, activation energies for the disappearance of all the enediynes are in excellent agreement with the activation energies derived from the appearance of the naphthalene products.

In general, the *para*-nitroenediynes is much better suited to be the reference point than 1,2-diethynylbenzene because it forms 2-nitronaphthalene cleanly and in a high yield²⁷ and because the presence of the *para*-NO₂ moiety at the para position approximates the electronic effect of the *ortho*-nitro group on the out-of-plane π system. A comparison of *para*- and *ortho*-nitroenediynes clearly confirms that it is not the presence of an acceptor substituent per se but its location that is of primary importance.

Generalized Kinetic Scheme for the Cycloaromatization Cascade. Although the usual focus of kinetic studies of the thermal reactivity of enediynes is on the Bergman cyclization, a number of further steps are needed to complete the cycloaromatization cascade, as illustrated in Scheme 3. The earlier observation that the cycloaromatization rate of benzannelated enediynes is sensitive to the 1,4-CHD concentration strongly suggests that these steps also contribute to the overall reaction kinetics.²⁸ Thus, we have chosen *para*-nitro and *ortho*-nitro benzannelated enediynes (2,3- and 3,4-diethynylnitrobenzenes) for a more detailed kinetic study aimed at the better understanding of the other steps in the cycloaromatization cascade.

The two steps of particular significance are the retro-Bergman cyclization, which is much faster in benzannelated enediynes²⁹ than in their acyclic analogues, and the first hydrogen abstraction step, which is decelerated by the loss of a through-bond (TB) interaction between the two radical centers.³⁰

When it is assumed that the major path for the consumption of nitroenediynes and the formation of nitronaphthalenes is the one depicted in Scheme 3 and that the formation of byproducts **D** is independent of the HD presence (e.g., the major byproducts are polymers from the reaction of *p*-benzynes with enediynes), the effective rate constant for the consumption of **A** and the formation of **C** can be described by eqs 3 and 4, respectively.⁵⁶

$$k_{\text{eff}}^{\text{A}} = \frac{k_1 k_2 [\text{HD}] + k_1 k_3}{k_2 [\text{HD}] + (k_{-1} + k_3)} = k_{\text{eff}}^{\text{C}} + k_{\text{eff}}^{\text{D}} = \frac{k_{\text{eff}}^{\text{C}}}{\text{yield}} \quad (3)$$

$$k_{\text{eff}}^{\text{C}} = \frac{k_1 k_2 [\text{HD}]}{k_2 [\text{HD}] + (k_{-1} + k_3)} \quad (4)$$

When the hydrogen abstraction step is much faster than the step leading to the byproducts **D**, $k_2[\text{HD}] \gg k_3$, one can reduce

TABLE 1. Effective Rate Constants for the Disappearance of Nitroenediynes ($k_{\text{eff}}^{\text{ED}}$) and the Appearance of Nitronaphthalenes ($k_{\text{eff}}^{\text{naphth}}$) at 140 °C^a

[1,4-CHD] (M)	<i>ortho</i> -NO ₂ enediynes ^b		<i>para</i> -NO ₂ enediynes ^c	
	$k_{\text{eff}}^{\text{ED}} \times 10^4$	$k_{\text{eff}}^{\text{naphth}} \times 10^4$	$k_{\text{eff}}^{\text{ED}} \times 10^4$	$k_{\text{eff}}^{\text{naphth}} \times 10^4$
0.73			1.85 ± 0.02	1.64 ± 0.01
0.58	6.98 ± 0.07	6.63 ± 0.06	1.68 ± 0.03	1.57 ± 0.01
0.44	6.44 ± 0.10	6.44 ± 0.03	1.60 ± 0.03	1.53 ± 0.01
0.29	5.74 ± 0.06	5.48 ± 0.01	1.48 ± 0.02	1.46 ± 0.01
0.15	4.31 ± 0.02	4.28 ± 0.02	1.22 ± 0.02	1.15 ± 0.01
0.07	3.06 ± 0.02	2.66 ± 0.01	0.99 ± 0.02	0.92 ± 0.02
0.03	2.23 ± 0.02	1.06 ± 0.02	0.73 ± 0.01	0.63 ± 0.01

^a Pseudo-first-order effective rate constants (k_{eff}) are in s⁻¹. ^b Initial concentration of enediynes = 2.7 × 10⁻³ M. ^c Initial concentration of enediynes = 3.8 × 10⁻³ M.

eqs 3 and 4 to eq 5. The latter can be rearranged to eq 6 which can be used to obtain k_1 graphically as the intercept of the plot of $1/k_{\text{eff}}$ versus $1/[\text{HD}]$:

$$k_{\text{eff}} = \frac{k_1 k_2 [\text{HD}]}{k_2 [\text{HD}] + k_{-1}} \quad (5)$$

$$\frac{1}{k_{\text{eff}}} = \frac{k_{-1}}{k_1 k_2 [\text{HD}]} + \frac{1}{k_1} \quad (6)$$

Effect of HD Concentration on the Effective Rate Constants. The above kinetic scheme has several verifiable consequences. First, it explains the effects of HD concentration on the rates of the Bergman cycloaromatization on a quantitative basis. Second, eq 6 allows one to recover the true first-order rate constants for the cyclization step using a simple graphical method. Most importantly, this scheme allows one to develop a general method for deconvoluting kinetic contributions from the individual steps in the overall kinetic scheme of the cycloaromatization cascade (k_1 , k_{-1} , k_2 , etc.). The key element in this development involved the analysis of the HD concentration effect on the overall reaction kinetics.

For a detailed mechanistic investigation of the Bergman cyclization, we have studied the effect of the concentration of the hydrogen-atom donor, 1,4-CHD, on the effective rate constant for the disappearance of enediynes and for the appearance of the corresponding naphthalene. 2,3-Diethynyl-nitrobenzene (*ortho*-NO₂) and 3,4-diethynylnitrobenzene (*para*-NO₂) were chosen as model compounds.

Rate constants for the disappearance of enediynes and the appearance of nitronaphthalenes at 140 °C are given in Table 1. Single-exponential decay (eq 1) was used to model the disappearance of enediynes with $R^2 > 0.9$, while linear correlation based on eq 2 was applied to the appearance of naphthalene. The effective rate constants (k_{eff}), determined from monitoring the disappearance of enediynes, include the rates of the Bergman cyclization, the retro-Bergman ring opening, and the hydrogen abstraction steps in addition to other reactions that do not lead to the naphthalene products. On the other hand, the effective rate constants (k_{eff}) determined from monitoring

(54) According to the ¹H NMR spectra, the major byproducts do not have aldehyde functionality but incorporate the modified 1,4-CHD moiety.

(55) Several of these rates even become slightly larger than the rates of the enediyne disappearance, and the result would be physically impossible if it were outside the error margins.

(56) Derivations of the rate equations are given in Supporting Information.

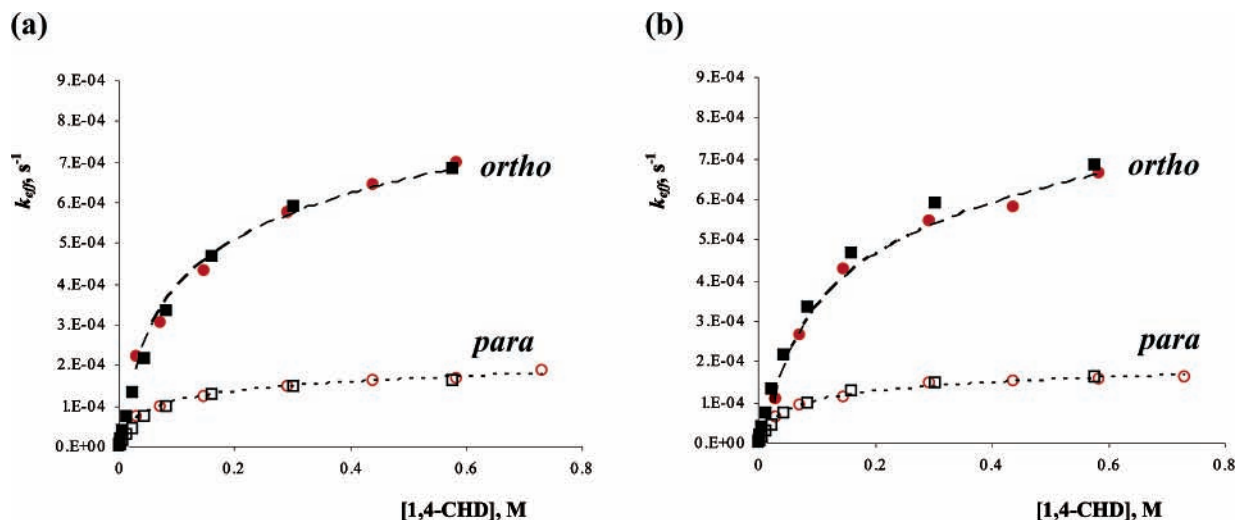


FIGURE 6. Dependence of effective rate constant, k_{eff} , from 1,4-CHD concentration at 140 °C; (a) disappearance of enediynes and (b) appearance of nitronaphthalenes. Filled red circles are data for *ortho*-nitroenediynes and hollow red circles are data for *para*-nitroenediynes; eq 5 was used to fit the data (filled black squares and hollow squares) when $k_1 = 8.3 \times 10^{-4} \text{ s}^{-1}$ and $k_{-1}/k_2 = 0.125 \text{ M}$ for *ortho*-nitro and $k_1 = 1.8 \times 10^{-4} \text{ s}^{-1}$ and $k_{-1}/k_2 = 0.067 \text{ M}$ for *para*-nitro.

TABLE 2. Activation Energies E_a Determined from Effective Rate Constants for the Consumption of NO_2 Enediynes and the Appearance of Nitronaphthalenes at Different Concentrations of [1,4-CHD]^a

[1,4-CHD] (M)	E_a for <i>ortho</i> - NO_2 enediynes ^b		E_a for <i>para</i> - NO_2 enediynes ^c	
	disappearance of enediynes	appearance of naphthalene	disappearance of enediynes	appearance of naphthalene
0.73			24.8 ± 0.3	24.9 ± 0.8
0.58	23.2 ± 0.5	24.0 ± 0.3	25.0 ± 0.4	25.2 ± 0.6
0.44	21.7 ± 0.1	22.8 ± 1.3	24.0 ± 0.8	23.4 ± 0.9
0.29	21.5 ± 0.1	21.0 ± 0.9	23.9 ± 0.3	22.8 ± 0.9
0.15	20.5 ± 0.1	19.6 ± 0.7	22.9 ± 0.4	23.5 ± 0.5
0.07	19.6 ± 0.9	20.9 ± 2.8	22.1 ± 0.5	22.9 ± 2.3
0.03	19.1 ± 0.4	19.8 ± 2.0	22.2 ± 0.6	23.2 ± 4.8

^a Activation energies in kcal/mol. ^b Initial concentration of enediynes = $2.7 \times 10^{-3} \text{ M}$. ^c Initial concentration of enediynes = $3.8 \times 10^{-3} \text{ M}$.

the appearance of naphthalene products comprise only the steps en route to the naphthalene product.

Both the effective rate constants for the consumption of enediynes and the formation of nitronaphthalene showed a dependence on the concentration of the hydrogen-atom donor that is qualitatively similar to that of the literature dependence for 1,2-diethynylbenzene.²⁸ A plot of the effective rate constants versus the 1,4-CHD concentration is shown in Figure 6. At low concentrations of 1,4-CHD, the effective rate constants for the consumption of enediynes are highly dependent on the concentration of 1,4-CHD. However, this dependence is less pronounced at higher concentrations of the HD, where the reaction rate finally reaches a plateau, as reported earlier for other enediynes.²⁸ A similar behavior is observed for the effective rate constants for the formation of nitronaphthalene.

Effective rate constants at different temperatures allowed us to determine Arrhenius activation energies at different concentrations of 1,4-CHD. The measured effective activation barriers are given in Table 2. An increase in the concentration of 1,4-CHD increases the activation energies for both nitroenediynes, but the *ortho* isomer is more sensitive to the 1,4-CHD concentration effect. At all concentrations of 1,4-CHD, correlations for effective rate constants for the consumption of enediynes are good, with less than ± 1 kcal/mol error in respect to the Arrhenius activation energies. On the other hand, effective rate constants for the formation of naphthalene products are

scattered when the concentration of 1,4-CHD is low. Consequently, activation energies for the appearance of nitronaphthalenes at 0.07 and 0.03 M 1,4-CHD have error bars in the order of ± 2.0 – 4.8 kcal/mol. These results are consistent with the change in the main reaction path from the Bergman cycloaromatization to the polymerization and formation of byproducts **D** at the lower concentrations. At a low concentration of 1,4-CHD, the effective rate constant in eq 3 transforms to that of eq 7 (see Supporting Information), which is based mainly on the rate constants of the path leading to the formation of byproducts **D**. Table 2 suggests that the activation energies for the formation of byproducts **D** are *less* than 19.1 and 22.1 kcal/mol for *ortho*- NO_2 and *para*- NO_2 enediynes, respectively. Because these values are lower than the activation barriers for the Bergman cyclization, the side reactions are unlikely to involve *p*-benzynes. Instead, chain polymerization is a reasonable possibility.⁴⁷

Dissection of Kinetics. Because the HD concentration effects on the activation barriers derived from the pseudo-first-order approximation can lead to noticeable discrepancies between the results from different sources and methods, it is beneficial to determine the true rate of the first-order cyclization constants, k_1 . In the following section, we will outline a simple way to determine these constants, which provide the real activation energies for the Bergman cyclization.

TABLE 3. Rate Constants at 140 °C Determined Using Equations 5 and 6^a

	<i>ortho</i> -NO ₂		<i>para</i> -NO ₂	
	disappearance of enediyne	appearance of naphthalene	disappearance of enediyne	appearance of naphthalene
		Equation 5		
$k_1 \times 10^4$ (s ⁻¹)	8.52 ± 1.33	7.97 ± 2.22	1.88 ± 1.11 ^b	1.79 ± 1.00
$k_{-1}/k_2 \times 10^2$ (M)	13.78 ± 2.12	13.63 ± 2.40	6.15 ± 1.56 ^b	7.25 ± 2.01
R^2	0.997	0.984	0.951	0.990
		Equation 6		
$k_1 \times 10^4$ (s ⁻¹)	8.26 ± 0.23	8.27 ± 0.49	1.87 ± 0.07	1.76 ± 0.04
$k_{-1}/k_2 \times 10^2$ (M)	12.58 ± 0.02	15.11 ± 0.10	6.82 ± 0.06	6.86 ± 0.41
R^2	0.997	0.991	0.974	0.989

^a The lowest 1,4-CHD concentration (0.03 M) was not included in the fit, unless otherwise noted. ^b Data for 0.03 M 1,4-CHD was included.

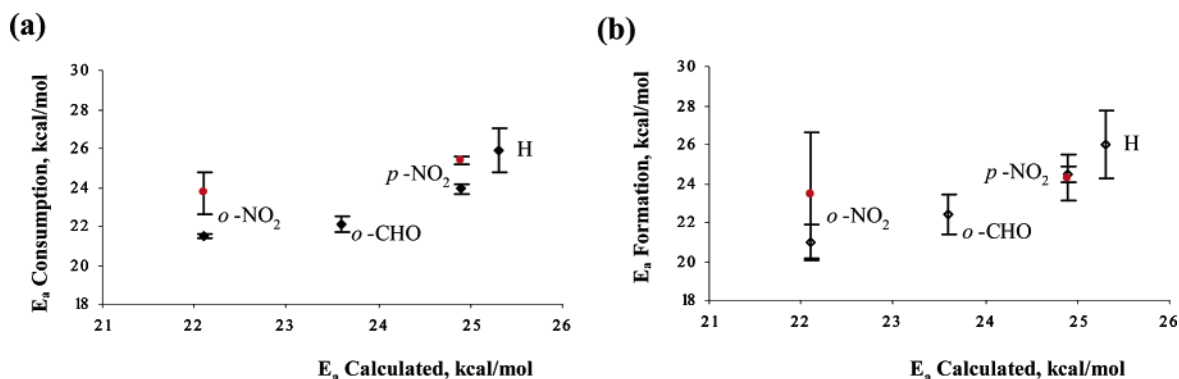


FIGURE 7. Correlation between activation energies calculated using UMP2 with the 6-31G(d,p) basis set and activation energies determined for (a) the consumption of enediynes and (b) the formation of the corresponding naphthalene products. Activation energies determined from the Bergman cyclization rate constants, k_1 , are shown in filled red circles.

Both k_1 and the k_{-1}/k_2 ratio can be determined either by multicomponent fitting of the data to eq 5 or by the graphical method based on eq 6. Table 3 compares the k_1 and the k_{-1}/k_2 values obtained by these two methods for the two nitroenediynes.

The above results suggest that only at a 1,4-CHD concentration of 0.14 M do the rates of the hydrogen abstraction reach that of the retro-Bergman opening and, thus, half of the *ortho*-nitro-*p*-benzyne intermediate is intercepted before reverting to the starting material. Such trapping is more efficient in the case of the *para*-nitro substrate, where a 50/50 threshold is achieved at a twofold smaller concentration of the H donor. One can attribute this difference to the steric effect of the nitro group in *ortho*-enediyne, which hinders the approach of 1,4-CHD from one side of the *p*-benzyne (syn to the nitro substituent). The difference in the rates of the retro-Bergman processes for the two *p*-benzynes may also be important. In both cases, a change to the rate-limiting step occurs at the steep part of the slope at approximately $1/2$ of the plateau height, as expected from the qualitative reasoning.

The final Arrhenius activation energies determined from k_1 (the true rate constant of the Bergman cyclization step) for the consumption of *ortho*- and *para*-NO₂ enediynes are 23.7 ± 1.1 and 25.4 ± 0.2 kcal/mol, whereas the activation energies determined from the formation of the nitronaphthalene products are 23.4 ± 3.2 and 24.3 ± 1.2 kcal/mol, respectively. These activation energies compare favorably with the activation energies determined from the effective rate constants, k_{eff} , at high 1,4-CHD concentrations. Although these values should be more accurate than all of the previous results, accuracy here is achieved at the expense of precision and, thus, the uncertainty of the measurements increases. Nevertheless, the difference in

the activation energies between *ortho*-NO₂ and *para*-NO₂ enediynes unequivocally supports the earlier computational prediction of the ortho effect in the Bergman cyclization.³¹

Discussion of Substituent Effects. First, the DSC data should be used with care and only for the most general qualitative assessments of reactivity. The perfect fit of DSC results for acceptor substituents discussed earlier in this paper is likely to be fortuitous because the DSC data are inconsistent with the results obtained from the classic kinetic approach either under pseudo-first-order conditions or using multicomponent kinetic dissection that recovers k_1 . At this stage, results based on multicomponent analysis have significant error margins. Therefore, our discussion will concentrate on results from the pseudo-first-order analysis. Encouragingly, the activation energies for the disappearance of enediynes with acceptor substituents and the appearance of the corresponding naphthalenes generally agree with each other (Figure 7). This observation suggests kinetically well-defined processes, further justifying the pseudo-first-order approximation.

Because cycloaromatization reactions provide a popular testing ground for the development of computational methods, in particular, different variations of DFT functionals,⁵⁷ it is interesting to comment on the performance of the two most commonly used functionals (BLYP vs B3LYP) for these reactions and investigate whether better alternatives are available for the computational description of such processes.

The *ortho*-NO₂ enediyne is indeed more reactive than the two reference enediynes unsubstituted at the ortho position. The 3.6–3.9 kcal/mol difference in the barriers for X = H agrees

(57) Prall, M.; Wittkopp, A.; Schreiner, P. R. *J. Phys. Chem. A* **2001**, *105*, 9265.

TABLE 4. Comparison of Activation Parameters from DFT Computations and from DSC Experiments^a

X	activation energies (kcal/mol)			pre-exponential factor log[A] (s ⁻¹)	
	BLYP (B3LYP) ^b	neat ED	in 1,4-CHD	neat ED	in 1,4-CHD
H	24.5 (31.3)	21.7 ± 0.3	23.1 ± 0.1	10.8 ± 0.3	10.0 ± 0.1
<i>ortho</i> -NO ₂	20.9 (27.9)	23.2 ± 0.1	22.0 ± 0.6	11.9 ± 0.1	10.3 ± 0.6
<i>para</i> -NO ₂	24.1 (30.9)	25.8 ± 0.3	25.9 ± 0.3	12.6 ± 0.2	10.8 ± 0.3
<i>ortho</i> -CHO (syn)	20.6 (27.7)	24.4 ± 0.2	23.2 ± 0.3	12.6 ± 0.2	10.8 ± 0.3
<i>ortho</i> -CHO (anti)	22.1 (29.2)				

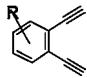
^a Errors are standard deviations of the Arrhenius fits with 90% confidence limits. ^b 6-31G** basis set.

TABLE 5. MP2/6-31G** Activation Energies, Experimental Activation Parameters Derived from Pseudo-First-Order Experiments, and Experimental Yields of 1-Substituted Naphthalenes^a

X	MP2 ^b	activation energies (kcal/mol)		pre-exponential factor log[A] (s ⁻¹)		yield (%)
		enediyne consumption	naphthalene formation	enediyne consumption	naphthalene formation	
H	25.3	25.9 ± 1.1	26.0 ± 1.7	9.4 ± 0.6	7.8 ± 0.8	35
<i>ortho</i> -NO ₂	22.1	21.5 ± 0.1	21.0 ± 0.9	8.2 ± 0.1	7.9 ± 0.5	75
<i>para</i> -NO ₂	24.9	23.9 ± 0.3	24.5 ± 0.4	8.8 ± 0.2	9.0 ± 0.2	70
<i>ortho</i> -CHO (syn)	22.1	22.1 ± 0.4	22.4 ± 1.0	7.9 ± 0.5	8.4 ± 0.5	48
<i>ortho</i> -CHO (anti)	23.6					

^a Errors are standard deviations of the Arrhenius fits with 90% confidence limits. ^b 6-31G** basis set.

TABLE 6. Comparison of Substituent Effects on the Stability of Reactants, TS, and Products of the Bergman Cyclization and Related Naphthalene Monoradicals at the BLYP (B3LYP) [MP2]/6-31G** Levels^a

	δE_R	δE_{TS}	δE_P	δE_{MR}
NO ₂	5.40 (5.83) [4.91]	2.19 (2.84) [2.22]	1.20 (2.06)	(2.08) [2.49]
CHO (syn)	3.85 (3.88) [3.32]	0.19 (0.54) [0.47]	2.17 (0.50)	(0.01) [1.06]
CHO (anti)	1.19 (1.25) [0.39]	-0.91 (-0.60) [-1.02]	1.26 (-0.40)	(0.62) [1.38]

^a Para-substituted isomers are taken as the reference points; positive values indicate destabilization by the ortho substituent.

well with the 3.4–3.6 kcal/mol DFT predictions (Table 4). The 2 kcal/mol barrier decrease for the *para*-NO₂ substrate is slightly lower than the approximately 3 kcal/mol DFT prediction, but this difference is well within the experimental error.

These results parallel the thermal behavior of *ortho*-CHO substituted enediyne, where the activation barriers determined by the three methods (Tables 4 and 5) are again within the experimental error. One has to mention that the rates were less accurate in this case because the data are more scattered as a result of the presence of side reactions and a lower yield of the naphthalene product. In addition, we did not study the effect of 1,4-CHD on the cyclization kinetics in this case. As a result, the activation barriers may be underestimated, explaining why the barrier lowering relative to X = H is more than expected from the DFT computations. Nevertheless, the Arrhenius fits at 0.27 M 1,4-CHD are acceptable and the 1.8–2 kcal/mol difference relative to the *para*-NO₂ enediyne agrees with the DFT prediction (Table 4) rather well.

From a practical point of view, an interesting observation is that, in some cases, the best fit to the experimentally determined activation energies is provided not by DFT but by MP2 calculations. The advantage of MP2 in such cases is likely to be a better description of the noncovalent interactions responsible for the ortho effect. Although unrestricted Møller–Plesset second-order perturbation theory (UMP2) performs poorly in the description of *p*-benzynes, it has been shown before that the TS of the Bergman cyclization is reactant-like with little diradical character.^{19,20} As a result, MP2 can be used to

determine the activation energies and may have an edge over DFT when noncovalent interactions contribute to the barrier variations. Table 6 illustrated the difference between DFT and MP2 methods in the description of the substituent effects where such direct through-space interactions are important. The steric destabilization of the reactants is noticeably reduced at the MP2 level, while the TSs have similar absolute energies (Table 5). We did not attempt a comparison of the two methods toward *p*-benzyne products as a result of the known difficulties in describing multiconfigurational wave functions of singlet diradicals. On the other hand, the comparison of the respective monoradicals is possible and suggests a lesser decrease in the steric destabilization at the MP2 level relative to the unrestricted DFT data. Together, lesser destabilization of the reactant and greater destabilization of the product result in a 0.9–1.6 kcal/mol increase in the reaction endothermicity and the attenuation of the ortho effect. Such differences between DFT and MP2 may become important for the accurate computational predictions of the activation barriers of the Bergman cyclizations of designed enediynes.

Conclusion

The experimental results presented in this work confirm earlier computational predictions of the ortho effect in benzannulated enediynes. Both *ortho*-NO₂ and *ortho*-CHO substituents substantially accelerate the Bergman cyclization. In particular, the difference in the activation energies for *ortho*-

and *para*-nitroenediynes is in excellent agreement with the difference in the activation barriers calculated at the BLYP/6-31G** and BLYP/6-31G* levels. The absolute values of the BLYP activation energies are closer to the respective experimental barriers. Interestingly, the MP2/6-31G** level that is not commonly used for theoretical studies on the Bergman cyclization provides results that generally rival and, in some cases, have a slight edge over the BLYP performance. We suggest that MP2 is a reasonable alternative to DFT in those cases where an accurate description of the contribution of the noncovalent interactions to the activation energy is needed.

The acceptor substitution alleviates complications from the competing radical reactions, allowing for a more accurate analysis of kinetic trends. The plots of the effective rate constant k_{eff} for the consumption of enediynes and for the formation of the naphthalene products versus changes in the 1,4-CHD concentration initially show a steep increase in the rates, which is followed by a plateau at the higher concentrations of the HD. At the lower HD concentrations, other reaction pathways successfully compete with cycloaromatization. The cyclization becomes the rate-limiting step at a threshold 1,4-CHD concentration that is unique for each enediyne. Thus, a thorough understanding of H-atom donor effects is important for accurate kinetic studies of reversible Bergman cyclizations where the dissection of reaction kinetics on the basis of a simple model allows one to recover the true first-order rate constants.

Computational Details

All reactant, product, and TS geometries involved in Bergman cyclizations were optimized at the UB3LYP/6-31G**, UBLYP,⁵⁸ UMP2, and MP2 levels using Gaussian 98 and Gaussian 03 programs.⁵⁹ The TS wave functions were identical at UMP2 and MP2 levels. From frequency computations, we confirmed that all transition structures had a single imaginary frequency.

Experimental Section

3-Nitrophenol, 1,2-dibromobenzene, trifluoromethanesulfonic anhydride, trimethylsilylacetylene, and 2,3-dihydroxy-1-formylbenzene are commercially available and were used as received. 1,4-CHD was distilled before use. 1,2-Diethynylbenzene⁴⁶ and 2,3-diethynylanisole³¹ were prepared according to the literature procedures. Capillaries (300-mm length, 1.5–1.8-mm outer diameter, 0.2-mm wall) used in kinetic studies were purchased from a commercial supplier.

Synthetic Procedures. Synthesis of 3-Formyl-phenyl-1,2-bis-(trifluoromethanesulfonate), 5. 2,3-Dihydroxy-1-formylbenzene (0.50 g, 3.62 mmol) and pyridine (1.5 mL, 18.1 mmol) were dissolved in CH₂Cl₂ (25 mL). The mixture was cooled to 0 °C under argon, and trifluoromethanesulfonic anhydride (1.4 mL, 8.0 mmol) was added dropwise. The reaction was slowly warmed to room temperature and stirred for 6 h. The mixture was diluted with CH₂Cl₂, washed with water, and dried over Na₂SO₄. The solvent was removed under vacuo. The reaction mixture was purified by chromatography on silica gel (10% ethyl acetate/hexanes) to afford 1.82 g (98%) of the desired product as a white solid: mp 38 °C.

(58) (a) Becke, A. D. *Phys. Rev. A: At., Mol., Opt. Phys.* **1988**, *38*, 3098. (b) Lee, C. T.; Yang, W. T.; Parr, R. G. *Phys. Rev. B: Condens. Matter* **1988**, *37*, 785. (c) Stephens, P. J.; Devlin, F. J.; Chabalowski, C. F.; Frisch, M. J. *J. Phys. Chem.* **1994**, *98*, 11623.

(59) (a) Frisch, M. J.; Et al. *Gaussian 98*, revision A.9; Gaussian, Inc.: Pittsburgh, PA, 1998. (b) Frisch, M. J.; Et al. *Gaussian 03*, revision C.01; Gaussian, Inc.: Wallingford, CT, 2004 (see Supporting Information for the complete references).

¹H NMR (300 MHz, CDCl₃): δ 10.2 (s, 1H), 8.0 (dd, 1H, *J* = 7.5, 1.5 Hz), 7.8 (dd, 1H, *J* = 8.1, 1.2 Hz), 7.7 (dd, 1H, *J* = 8.1, 7.8 Hz). ¹³C NMR (75.5 MHz, CDCl₃): δ 185.0, 141.1, 140.2, 131.0, 130.2, 129.8, 128.5, 118.3 (q, *J* = 321.2 Hz), 118.2 (q, *J* = 321.8 Hz). UV/vis (CH₃CN): λ_{max} (log ε) 280 (3.18), 238 (3.85), 203 (4.54) nm. IR (neat): 3401, 3094, 2888, 2758, 1709, 1432, 1223, 1210, 1129, 958, 873 cm⁻¹. HRMS (EI⁺): calcd for C₉H₄O₇F₆S₂, 401.930 25; found, 401.929 98.

General Procedure for Sonogashira Coupling. A suspension of aryl dihalide or ditriflate (5.8 mmol), PdCl₂(PPh₃)₂ (0.29 mmol), and Cu(I) iodide (0.29 mmol) in 40 mL of amine solvent was degassed three times with the freeze/pump/thaw technique in a flame-dried, screw-cap, pressure tube. Trimethylsilylacetylene (14.5 mmol) was added using a syringe. The tube was capped, and the mixture was heated in an oil bath equipped with a thermostat. The reaction progress was monitored by TLC. After the total consumption of the aryl halide, the reaction mixture was filtered through Celite and washed with methylene chloride (3 × 30 mL). The organic layer was washed with a saturated solution of ammonium chloride (2 × 30 mL) and water (2 × 30 mL) and dried over anhydrous Na₂SO₄. The solvent was removed in vacuo. The reaction mixture was purified by flash chromatography on silica gel.

Synthesis of 2,3-Bis(trimethylsilylethynyl)nitrobenzene, 6. The title compound was prepared by the Sonogashira coupling of 2,3-dibromonitrobenzene (2.2 g, 7.8 mmol) with trimethylsilylacetylene (1.92 g, 19.6 mmol) in 60 mL of (*i*-Pr)₂NH at 95 °C for 24 h. The reaction mixture was purified by flash chromatography on silica gel (hexanes) to afford 1.85 g (72%) of the desired product as a brown solid: mp 67–68 °C. ¹H NMR (300 MHz, CDCl₃): δ 7.86 (d, 1H, *J* = 7.5 Hz), 7.68 (dd, 1H, *J* = 8.1 Hz), 7.36 (dd, 1H, *J* = 8.1, 7.5 Hz), 0.28 (s, 9H), 0.27 (s, 9H). ¹³C NMR (75.5 MHz, CDCl₃): δ 150.9, 136.2, 128.8, 127.7, 123.7, 120.0, 108.6, 101.4, 101.1, 97.0, -0.5, -0.7. UV/vis (CH₃CN): λ_{max} (log ε) 328 (4.28), 264 (4.20), 250 (4.48), 214 (4.49) nm. IR (neat): 2962, 2900, 2164, 1532, 1353, 1248, 846, 761 cm⁻¹. HRMS (EI⁺): calcd for C₁₆H₂₁NO₂Si₂, 315.111 09; found, 315.111 04.

Synthesis of 3,4-Bis(trimethylsilylethynyl)nitrobenzene, 7. The title compound was prepared by the Sonogashira coupling of 3,4-dibromonitrobenzene (3.1 g, 9.8 mmol) with trimethylsilylacetylene (2.41 g, 24.6 mmol) in 60 mL of (*i*-Pr)₂NH at 110 °C for 24 h. The reaction mixture was purified by flash chromatography on silica gel (hexanes) to afford 2.78 g (80%) of the desired product as an off-white solid: mp 118–121 °C. ¹H NMR (300 MHz, CDCl₃): δ 8.3 (d, 1H, *J* = 2.4 Hz), 8.0 (dd, 1H, *J* = 9.0, 2.7 Hz), 0.29 (s, 18H). ¹³C NMR (75.5 MHz, CDCl₃): δ 146.9, 133.2, 132.1, 127.4, 127.3, 122.8, 105.1, 102.0, 101.6, 101.1, 0.03, -0.01. UV/vis (CH₃CN): λ_{max} (log ε) = 307 (4.17), 261 (4.34), 229 (4.27), 220 (4.28) nm. IR (neat): 3280, 3106, 2110, 1573, 1522, 1354, 909, 661 cm⁻¹. HRMS (EI⁺): calcd for C₁₆H₂₁NO₂Si₂, 315.111 09; found, 315.110 16.

Synthesis of 2,3-Bis(trimethylsilylethynyl)-1-formylbenzene, 8. The title compound was prepared by the Sonogashira coupling of 3-formyl-phenyl-1,2-bis(trifluoromethanesulfonate) (0.70 g, 1.74 mmol) with trimethylsilylacetylene (0.41 g, 4.18 mmol) in 20 mL of dry THF and with K₂CO₃ (1.2 g, 8.71 mmol) as the base at 110 °C for 8 h. The reaction mixture was purified by flash chromatography on silica gel (1% ethyl acetate/hexanes) to afford 0.28 g (54%) of the desired product: ¹H NMR (300 MHz, CDCl₃): δ 10.5 (s, 1H), 7.8 (d, 1H, *J* = 7.5 Hz), 7.7 (d, 1H, *J* = 7.5 Hz), 7.3 (dd, 1H, *J* = 8.1, 7.2 Hz), 0.28 (s, 9H), 0.27 (s, 9H); ¹³C NMR (75.5 MHz, CDCl₃) δ 191.4, 137.2, 136.2, 128.8, 127.9, 127.4, 126.4, 106.9, 101.7, 100.1, 97.9, -0.4, -0.5. UV/vis (CH₃CN): λ_{max} (log ε) 322 (3.07), 284 (3.79), 253 (4.31) nm; IR (neat) 2956, 2846, 2361, 2336, 1699, 1559, 1250, 844 cm⁻¹. HRMS (EI⁺) calcd for C₁₇H₂₂OSi₂, 298.120 93; found, 298.120 17.

General Procedure for TMS Deprotection. An aliquot of 1 N NaOH (5 mL) was added to a methanol solution (50 mL) of enediyne (3.2 mmol). The mixture was stirred at room temperature for 15 min. The progress of the reaction was monitored by TLC.

After the total transformation of the TMS acetylenes, the solvent was removed in vacuo. Aqueous HCl (1 N, 10 mL) was added to the crude mixture. The acidic mixture was extracted by dichloromethane (3 × 20 mL). The organic layer was washed with water (2 × 30 mL) and dried over anhydrous Na₂SO₄. The solvent was removed in vacuo. The reaction mixture was purified by flash chromatography on silica gel.

Synthesis of 2,3-Diethynylnitrobenzene (*ortho*-NO₂ Ene-diyne), 2. The title compound was prepared by the TMS deprotection of 2,3-bis(trimethylsilylethynyl)nitrobenzene (1.01 g, 3.21 mmol) with 1 N NaOH (5 mL) in 50 mL of MeOH at room temperature for 15 min. The reaction mixture was purified by flash chromatography on silica gel (hexanes) to afford 0.49 g (90%) of the desired product as a white solid: mp 84 °C. ¹H NMR (300 MHz, CDCl₃): δ 7.9 (d, 1H, *J* = 8.1 Hz), 7.7 (d, 1H, *J* = 8.1 Hz), 7.4 (dd, 1H, *J* = 8.1), 3.8 (s, 1H), 3.4 (s, 1H). ¹³C NMR (75.5 MHz, CDCl₃): δ 151.0, 136.6, 128.5, 128.4, 124.2, 119.6, 89.7, 83.7, 79.9, 76.2. UV/vis (CH₃CN): λ_{max} (log ε) 330 (2.98), 282 (3.85), 261 (4.07), 228 (4.05) nm. IR (neat): 3276, 2105, 1517, 1352, 741 cm⁻¹. HRMS (EI⁺): calcd for C₁₀H₅O₂N, 171.032 03; found, 171.032 11.

Synthesis of 3,4-Diethynylnitrobenzene (*para*-NO₂ Ene-diyne), 3. The title compound was prepared by the TMS deprotection procedure of 3,4-bis(trimethylsilylethynyl)nitrobenzene (1.50 g, 4.76 mmol) with 1 N NaOH (10 mL) in 150 mL of MeOH at room temperature for 15 min. The reaction mixture was purified by flash chromatography on silica gel (hexanes) to afford 0.59 g (72%) of the desired product as a white solid: mp 92 °C. ¹H NMR (300 MHz, CDCl₃): δ 8.3 (d, 1H, *J* = 2.4 Hz), 8.1 (dd, 1H, *J* = 8.4, 2.4 Hz), 7.6 (d, 1H, *J* = 9.0), 3.6 (s, 1H), 3.5 (s, 1H). ¹³C NMR (75.5 MHz, CDCl₃): δ 147.3, 133.7, 131.4, 127.6, 126.8, 123.4, 86.6, 84.1, 80.4, 79.9. UV/vis (CH₃CN): λ_{max} (log ε) = 289 nm (4.13), 238 (4.26), 218 (4.30). IR (neat): 2960, 2899, 2145, 1523, 1346, 1248, 847 cm⁻¹. HRMS (EI⁺): calcd for C₁₀H₅O₂N, 171.032 03; found, 171.031 07.

Synthesis of 2,3-Diethynyl-1-formylbenzene (*ortho*-CHO Ene-diyne) 4. The title compound was prepared by TMS deprotection of 2,3-bis(trimethylsilylethynyl)-1-formylbenzene (0.50 g, 1.68 mmol) with K₂CO₃ (1.00 g) in 30 mL of MeOH at room temperature for 15 min. The reaction mixture was purified by flash chromatography on silica gel (hexanes) to afford 0.20 g (78%) of the desired product as a white solid: mp 113–114 °C. ¹H NMR (300 MHz, CDCl₃): δ 10.6 (s, 1H), 7.9 (dd, 1H, *J* = 7.8, 1.2 Hz), 7.7 (dd, 1H, *J* = 8.1, 1.2 Hz), 7.4 (dd, 1H, *J* = 8.1, 7.5), 3.7 (s, 1H), 3.4 (s, 1H). ¹³C NMR (75.5 MHz, CDCl₃): δ 190.9, 137.5, 136.7, 128.5, 127.9, 127.1, 126.9, 88.5, 82.5, 80.4, 77.0. UV/vis (CH₃CN): λ_{max} (log ε) 319 (3.00), 262 (4.03), 242 (4.54) nm. IR (neat): 3261, 2853, 2102, 1694, 1437, 1244, 794, 637 cm⁻¹. HRMS (EI⁺): calcd for C₁₁H₆O, 154.041 87; found, 154.042 08.

Representative Procedure for the Preparative Scale of Bergman Cyclizations. Ene-diyne (0.5 mmol) was dissolved in anhydrous chlorobenzene (9 mL). 1,4-CHD (50 mmol) was added, and the mixture was placed in a Pyrex glass tube equipped with a joint. The tube was attached through the joint to a vacuum line, and the mixture was degassed three times by the freeze/pump/thaw technique. The tube was sealed under argon, placed in an oil bath, and heated to the corresponding temperature. After cooling, chlorobenzene was distilled in vacuo, and the products were isolated and purified by chromatography.

Differential Scanning Calorimetry Studies. Temperature and enthalpy calibrations were performed using an indium standard. The heat capacity was calibrated using a 25-mg sapphire standard. About 8–10 mg of enediyne was used for each experiment. For neat samples, enediynes were sealed in aluminum hermetic pans. The samples were equilibrated in the purge gas (argon) for about 15 min prior to each run. For solution samples, stock solutions of enediynes (5.0 mg) in 1,4-CHD (0.5 mL) were prepared, and 50 μL of the stock solutions were sealed in high volume aluminum pans with O-rings in a glovebox under argon.

Conventional DSC was used to determine the reaction kinetics using ASTM E 698 thermal stability protocol.⁴³ This protocol is used to determine Arrhenius activation energies and pre-exponential factors.

Kinetic Studies. Kinetic Studies of 2,3-Diethynylnitrobenzene (*ortho*-NO₂). A 10 mL volumetric flask was charged with 2,3-diethynylnitrobenzene (3.8 mg), 1,2,3,4-tetraphenylnaphthalene (7.8 mg), and 1,4-CHD (0.22 M). The solution was mixed and analyzed with HPLC to determine the initial concentration of the enediynes (2.2 × 10⁻³ M). Kinetic experiments were performed at 140, 148, 156, and 164 °C. The following conditions were used for kinetic analysis using HPLC: A/B, 9:1 solvent system (A, hexanes; B, hexanes/ethyl acetate, 30:1); 1 mL/min flow rate; and 265 nm detector wavelength. Retention times were as follows: *t*_{std} = 6.9 min, *t*_{naphth} = 11.3, and *t*_{ED} = 21.5 min.

Kinetic Studies of 2,3-Diethynyl-1-formylbenzene (*ortho*-CHO). A 10 mL volumetric flask was charged with 2,3-diethynyl-1-formylbenzene (3.7 mg), 1,2,3,4-tetraphenylnaphthalene (5.3 mg), and 1,4-CHD (0.24 M). The solution was mixed and analyzed with GC and HPLC to determine the initial concentration of enediynes (2.4 × 10⁻³ M). Kinetic experiments were performed at 140, 150, 160, 170, and 180 °C. The GC time program had the following parameters: initial temperature = 70 °C for 5 min, 20 °C/min until 220 °C and hold for 5 min, then 50 °C/min until 320 °C and hold for 1 min. Retention times were as follows: *t*_{ED} = 4.7, *t*_{naphth} = 5.2, and *t*_{std} = 8.9 min. The following conditions were used for kinetic analysis using HPLC: A/B, 8:2 solvent system (A, hexanes; B, hexanes/ethyl acetate, 100:1); 1 mL/min flow rate; and 265 nm detector wavelength. Retention times were as follows: *t*_{std} = 8.5, *t*_{naphth} = 30.8, and *t*_{ED} = 33.8 min.

Kinetic Studies of 3,4-Diethynylnitrobenzene (*para*-NO₂). A 10 mL volumetric flask was charged with 3,4-diethynylnitrobenzene (6.5 mg), anthracene (10.5 mg), and 1,4-CHD (0.38 M). The solution was mixed and analyzed with HPLC to determine the initial enediyne concentration (3.80 × 10⁻³ M). Kinetic experiments were performed at 140, 150, 160, and 170 °C. The following conditions were used for kinetic analysis using HPLC (reverse phase): A/B, 3:7 solvent system (A, water; B, acetonitrile); 1 mL/min flow rate; and 315 nm detector wavelength. Retention times were as follows: *t*_{ED} = 5.8, *t*_{naphth} = 6.6, and *t*_{std} = 15.1 min.

Kinetic Studies under Different Concentrations of 1,4-CHD. Kinetic Studies of 2,3-Diethynylnitrobenzene (*ortho*-NO₂). A 10 mL volumetric flask was charged with 2,3-diethynylnitrobenzene (25.0 mg, 14.6 × 10⁻³ M) and 1,2,3,4-tetraphenylnaphthalene (25.0 mg). Five master solutions (2.9 × 10⁻³ M each) were prepared with different concentrations of 1,4-CHD, [1,4-CHD] = 0.03, 0.07, 0.15, 0.29, 0.44, and 0.58 M. The enediynes initial concentration for every stock solution was determined by GC and HPLC as 2.7 × 10⁻³ M. Kinetic experiments were performed at 140, 148, 156, and 164 °C. The following conditions were employed for kinetic analysis by HPLC: A/B, 9:1 solvent system (A, hexanes; B, hexanes/ethyl acetate, 30:1); 1 mL/min flow rate; and 265-nm detector wavelength. Retention times were as follows: *t*_{std} = 6.9, *t*_{naphth} = 11.3, and *t*_{ED} = 21.5 min.

Kinetic Studies of 3,4-Diethynylnitrobenzene (*para*-NO₂). A 10 mL volumetric flask was charged with 3,4-diethynylnitrobenzene (30.0 mg, 17.5 × 10⁻³ M) and anthracene (60.0 mg). Six master solutions (3.5 × 10⁻³ M each) were prepared with different concentrations of 1,4-CHD, [1,4-CHD] = 0.03, 0.07, 0.15, 0.29, 0.44, 0.58, and 0.87 M. The enediynes initial concentration for every stock solution was determined by GC and HPLC as 3.8 × 10⁻³ M. Kinetic experiments were performed at 140, 150, 160, and 170 °C. The following conditions were used for kinetic analysis using HPLC (C13 reverse phase column): A/B, 3:7 solvent system (A, water; B, acetonitrile); 1 mL/min flow rate; and 315 nm detector wavelength. Retention times were as follows: *t*_{ED} = 5.8, *t*_{naphth} = 6.6, and *t*_{std} = 15.1 min.

Acknowledgment. The authors are grateful to the National Science Foundation (CHE-0316598) and to Material Research and Technology (MARTECH) Center at Florida State University for partial support of this research, to the 3M Company for an Untenured Faculty Award, to the Florida State University Supercomputing Center and the National Center for Supercomputing Application (NCSA, UIUC) for providing computational facilities, and to Professor Jack Saltiel for helpful discussions. The authors are also thankful to Dr. Umesh Goli and Mr. Hank Henricks of the Biochemical Analysis and Synthesis Services

(BASS lab) of the Department of Chemistry and Biochemistry at Florida State University.

Supporting Information Available: Additional information including the general kinetic experimental setup and NMR spectra: ^1H and ^{13}C NMR. Computational details including complete geometries and absolute energies at all levels of theory. Complete ref 59. This material is available free of charge via the Internet at <http://pubs.acs.org>.

JO0520801